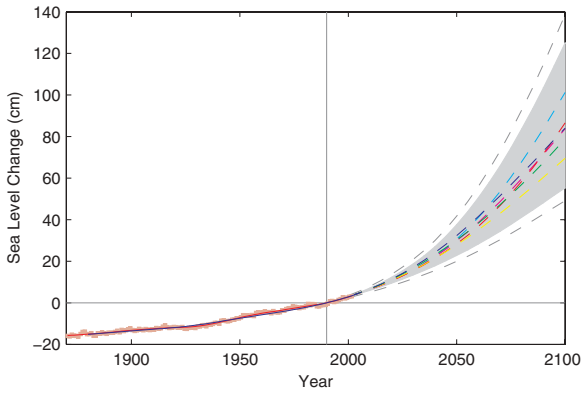

Fig. 4. Past sea level and sea-level projections from 1990 to 2100 based on global mean temperature projections of the IPCC TAR. The gray uncertainty range spans the range of temperature rise of 1.4° to 5.8° C, having been combined with the best statistical fit shown in Fig. 2. The dashed gray lines show the added uncertainty due to the statistical error of the fit of Fig. 2. Colored dashed lines are the individual scenarios as shown in (*1*); the light blue line is the A1FI scenario, and the yellow line is the B1 scenario.

linear approximation performs, although the approximation is frequently used by glaciologists ("degree-days scheme"). Given the dynamical response of ice sheets observed in recent decades and their growing contribution to overall sea-level rise, this approximation may not be robust. The ice sheets may respond more strongly to temperature in the 21st century than would be suggested by a linear fit to the 20th century data, if time-lagged positive feedbacks come into play (for example, bed lubrication, loss of buttressing ice shelves, and ocean warming at the grounding line of ice streams). On the other hand, many small mountain glaciers may disappear within this century and cease to contribute to sea-level rise. It is therefore difficult to say whether the linear assumption overall leads to an over- or underestimation of future sea level. Occam's razor suggests that it is prudent to accept the linear assumption as reasonable, although it should be kept in mind that a large uncertainty exists, which is not fully captured in the range shown in Fig. 4.

Regarding the lowest plausible limit to sea-level rise, a possible assumption may be that the rate shown in Fig. 3 stops increasing within a few years (although it is difficult to see a physical reason for this) and settles at a constant value of 3.5 mm/year. This implies a sea-level rise of 38 cm from 1990 to 2100. Any lower value would require that the rate of sea-level rise drops despite rising temperature, reversing the relationship found in Fig. 2.

Although a full physical understanding of sea-level rise is lacking, the uncertainty in future sea-level rise is probably larger than previously estimated. A rise of over 1 m by 2100 for strong warming scenarios cannot be ruled out, because all that such a rise would require is that the linear relation of the rate of sea-level rise and temperature, which was found to be valid in the 20th century, remains valid in the 21st century. On the other hand, very low sea-level rise values as reported in the IPCC TAR now appear rather implausible in the light of the observational data.

The possibility of a faster sea-level rise needs to be considered when planning adaptation measures, such as coastal defenses, or mitigation measures designed to keep future sea-level rise within certain limits [for example, the 1-m long-term limit proposed by the German Advisory Council on Global Change (*13*)].

References and Notes

1. J. T. Houghton *et al.*, Eds., *Climate Change 2001: The Scientific Basis* (Cambridge Univ. Press, Cambridge, 2001).
2. H. J. Zwally *et al.*, *Science* **297**, 218 (2002).
3. E. Rignot *et al.*, *Geophys. Res. Lett.* **31**, 18 (2004).
4. S. C. B. Raper, R. J. Braithwaite, *Nature* **439**, 311 (2006).
5. C. Waelbroeck *et al.*, *Quat. Sci. Rev.* **21**, 295 (2002).
6. T. Schneider von Deimling, A. Ganopolski, H. Held, S. Rahmstorf, *Geophys. Res. Lett.* **33**, L14709 (2006).
7. H. J. Dowsett *et al.*, *Global Planet. Change* **9**, 169 (1994).
8. J. A. Church, N. J. White, *Geophys. Res. Lett.* **33**, L01602 (2006).
9. J. Hansen *et al.*, *J. Geophys. Res. Atmos.* **106**, 23947 (2001).
10. P. D. Jones, M. E. Mann, *Rev. Geophys.* **42**, RG2002 (2004).
11. S. Jevrejeva, A. Grinsted, J. C. Moore, S. Holgate, *J. Geophys. Res.* **111**, 09012 (2006).
12. M. Montoya *et al.*, *Clim. Dyn.* **25**, 237 (2005).
13. German Advisory Council on Global Change, "The future oceans: warming up, rising high, turning sour," (Wissenschaftlicher Beirat der Bundesregierung Globale Umweltveränderungen Special Report, Berlin, 2006); (www.wbgu.de/wbgu_sn2006_en.pdf).
14. J. C. Moore, A. Grinsted, S. Jevrejeva, *Eos* **86**, 226 (2005).
15. The statistical error was calculated by means of the Matlab function "polyval" for the linear fit shown in Fig. 2.
16. The author thanks J. Church for providing the observational data and M. Stöckmann for the model data. They as well as J. Gregory and B. Hare are thanked for valuable discussions.

Supporting Online Material

www.sciencemag.org/cgi/content/full/1135456/DC1
Figs. S1 to S3

22 September 2006; accepted 4 December 2006
Published online 14 December 2006;
10.1126/science.1135456
Include this information when citing this paper.

Nonequilibrium Mechanics of Active Cytoskeletal Networks

Daisuke Mizuno,[1] Catherine Tardin,[1] C. F. Schmidt,[1,2]* F. C. MacKintosh[1]*

Cells both actively generate and sensitively react to forces through their mechanical framework, the cytoskeleton, which is a nonequilibrium composite material including polymers and motor proteins. We measured the dynamics and mechanical properties of a simple three-component model system consisting of myosin II, actin filaments, and cross-linkers. In this system, stresses arising from motor activity controlled the cytoskeletal network mechanics, increasing stiffness by a factor of nearly 100 and qualitatively changing the viscoelastic response of the network in an adenosine triphosphate–dependent manner. We present a quantitative theoretical model connecting the large-scale properties of this active gel to molecular force generation.

Mechanics directly control many functions of cells, including the generation of forces, motion, and the sensing of external forces (*1*). The cytoskeleton is a network of semiflexible linear protein polymers (actin filaments, microtubules, and intermediate filaments) that is responsible for most of the mechanical functions of cells. It differs from common polymer materials in both the complexity of composition and the fact that the system is not at thermodynamic equilibrium. Chemical nonequilibrium drives mechanoenzymes (motor proteins) that are the force generators in cells. The cytoskeleton is thus an active material that can adapt its mechanics and perform mechanical tasks such as cell locomotion or cell division.

Here, we show how nonequilibrium motor activity controls the mechanical properties of a simple three-component in vitro model cytoskeletal network. The nonequilibrium origin of this active control mechanism can be seen directly in the violation of a fundamental theorem of statistical physics, the fluctuation-dissipation (FD) theorem, which links thermal fluctuations of systems to their response to external forces. The FD theorem is a generalization of Einstein's description of Brownian motion (*2*). Although it is valid only in equilibrium, its possible extension to out-of-equilibrium systems such as granular materials and living cells has been debated (*3*–*5*). Prior studies in cells have suggested violations of the FD theorem (*3*), but this has not been directly observed. We show that an in vitro model system consisting of a cross-linked

[1]Department of Physics and Astronomy, Vrije Universiteit, 1081HV Amsterdam, Netherlands. [2]III. Physikalisches Institut, Fakultät für Physik, Georg-August-Universität, 37077 Göttingen, Germany.

*To whom correspondence should be addressed. E-mail: cfs@nat.vu.nl (C.F.S.); fcm@nat.vu.nl (F.C.M.)

actin network with embedded force-generating myosin II motors strongly violates the FD theorem and that it does so because of the contractility of the acto-myosin system.

Actin and myosin are key components in muscle contraction and cell motility (*6*, *7*). Myosin motor domains, or heads, bind to actin filaments (F-actin) and generate force via the hydrolysis of adenosine triphosphate (ATP), resulting in motion along the polar actin filaments. At low salt concentrations, myosin II can form multimeric bipolar structures in vitro (Fig. 1A) (*8*). These "minifilaments" can link different actin filaments and move these filaments relative to each other (*9*). In the absence of ATP, these motor complexes statically cross-link F-actin and generate bundles that can be seen in a light microscope (Fig. 1B). In the presence of ATP, minifilaments generate contractile forces that can result in actin aggregation and phase separation (Fig. 1C), a phenomenon known as superprecipitation (*10*). To stabilize the networks and delay the onset of superprecipitation, we used F-actin cross-linked by biotin and neutravidin.

We measured the mechanical properties of these networks by active microrheology (AMR) (*11*–*13*), in which micrometer-sized embedded probe particles are manipulated by a sinusoidally oscillated optical trap, generating a force F at frequency ω. The response function $\alpha(\omega)$ is obtained from the measured probe particle displacement $u(\omega)$:

$$\alpha(\omega) = u(\omega)/F \qquad (1)$$

For a simple incompressible and homogeneous elastic medium, this response function is related to the shear modulus G or stiffness of the medium via a generalization of the Stokes relation (*13*–*17*) $\alpha = 1/(6\pi G a)$, where a is the probe particle radius. For materials with dissipation, the displacement u and force F are not in phase, which results in a complex response function. In this case, the shear modulus is $G = G' + iG''$, where G' is the elastic modulus and G'' is the viscous modulus. For cross-linked actin (1 mg/ml) gels, we found a predominantly elastic response in which G' is much larger than G'' in the range of frequencies below 100 Hz. The measured moduli are consistent both with experiments on similar actin gels (*18*) and with theoretical predictions for actin networks with an average distance of about 2 to 3 μm between cross-links (*13*, *19*).

To characterize motor-generated activity, we used passive microrheology (PMR), which consists of recording the spontaneous displacement fluctuations of a probe particle without applied forces (*13*–*16*). In an equilibrium system, only thermal forces act on the probe, and the power spectral density

$$C(\omega) = \int \langle u(t)u(0) \rangle \exp(i\omega t)\, dt \qquad (2)$$

of the displacement fluctuations $u(t)$ is directly related to the mechanical response of the material by the FD theorem,

$$\alpha''(\omega) = \frac{\omega}{2k_B T} C_{eq}(\omega) \text{ (equilibrium only)} \qquad (3)$$

where $\alpha''(\omega)$ is the imaginary part of the response function, k_B is the Boltzmann constant, and T is absolute temperature. Because we can independently measure the left side of Eq. 3 with AMR and the right side with PMR, we can search for signatures of motor activity in the form of violations of the FD theorem.

As a control, we first verified the FD theorem as expressed in Eq. 3 for an equilibrium sample by directly comparing $\alpha''(\omega)$ measured with AMR and $\omega C(\omega)/2k_B T$ measured with PMR. For cross-linked actin without myosin, the agreement with Eq. 3 is shown in Fig. 2A.

Active processes create additional fluctuations and are expected to make the right side of Eq. 3 larger than the left side, thus violating the FD theorem. Indirect evidence for this has been reported in cells (*3*). We started with experiments at 3.5 mM ATP, where motors are expected to be active. Interestingly, we saw no difference between AMR and PMR results for up to 5 hours (Fig. 2A). At longer times, however, a clear difference developed in the form of strongly enhanced fluctuations at frequencies below 10 Hz (Fig. 2B). The appearance of these nonequilibrium fluctuations after a time lag can be explained by a switching of the myosin minifilaments from a nonprocessive mode, which cannot generate forces between actin filaments, to a processive tension-generating mode. Such a transition is expected because the ratio of attached to unattached time (duty ratio) of myosin increases with decreasing ATP concentration, when motor release induced by ATP binding becomes the rate-limiting step in the chemical cycle (*20*). Consistent with this, the lag time increased with increasing initial ATP concentra-

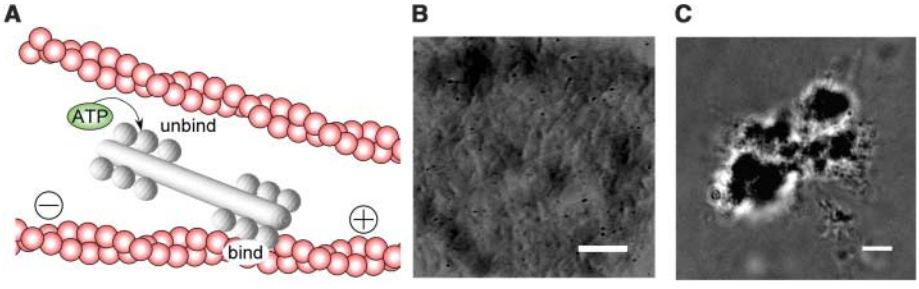

Fig. 1. (**A**) Schematic of a bipolar myosin filament interacting with two actin filaments. Polarity of actin is indicated by the +/– signs (myosin moves toward the plus end). (**B**) Differential interference contrast microscopy image of bundled actin filaments at high salt concentration ([KCl] = 150 mM, actin concentration 1 mg/ml, myosin concentration 170 nM, no cross-links). As ATP depletes, thick acto-myosin bundles form without phase separation. (**C**) At low salt concentration ([KCl] = 50 mM), active myosin filaments result in contraction of the actin network to form dense acto-myosin aggregates (superprecipitation). Scale bars, 5 μm.

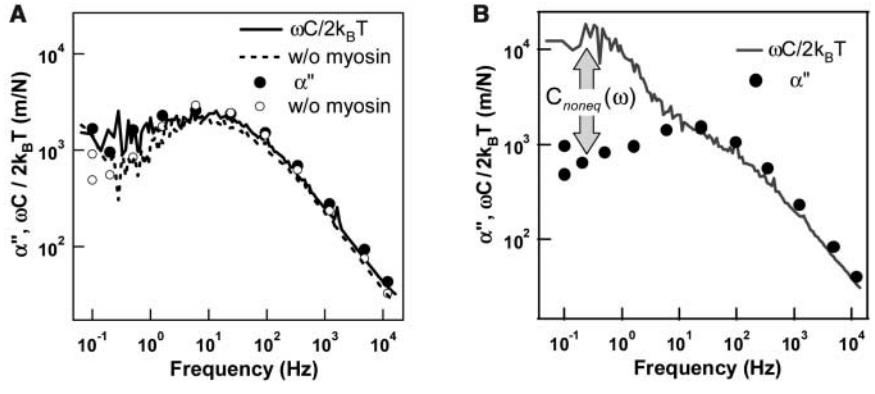

Fig. 2. Mechanical response of cross-linked nonactive and active gels (actin and myosin concentrations as in Fig. 1). (**A**) The imaginary part of the response function α'' measured by AMR (circles) and the normalized power spectrum $\omega C(\omega)/2k_B T$ measured by PMR (lines). Open circles and the dashed line denote cross-linked actin without myosin; solid circles and the solid line denote networks with myosin 2.5 hours after sample preparation. For up to 5 hours, α'' and $\omega C(\omega)/2k_B T$ with and without myosin show good agreement, indicating that myosin activity did not yet produce observable nonequilibrium fluctuations. (**B**) The same as (A) but 6.8 hours after sample preparation (with myosin). Below 10 Hz, nonequilibrium fluctuations are observable as an enhancement of $\omega C(\omega)/2k_B T$ relative to α''.

tion. We also performed experiments at low ATP concentrations stabilized with an ATP regenerating system (*13*). At ATP concentrations below ~60 μM, we observed stable active fluctuations in the gels lasting for several hours.

Along with the nonequilibrium fluctuations, we saw a strong stiffening of the networks due to motor activity. This is apparent in the reduced response or compliance of the network (Fig. 3A). The shear modulus can be calculated using the generalized Stokes formula (*14*–*17*) (Fig. 3B). Here, the network stiffness increases by a factor of almost 100 depending on the ATP concentration. The stiffening of the network is related to the well-known strain stiffening response of actin gels under external stress (*18*, *19*, *21*): The contractile activity of motors results in internal tensile stresses in the actin filaments, which make the network more rigid. Unlike stiffening due to anisotropic shear stress, however, we expect that stresses induced by the motors are isotropic, which should lead to more pronounced stiffening because filaments of all orientations can participate.

The hypothesis that the observed stiffening is due to isotropically tensed filaments can be tested quantitatively by an examination of the frequency dependence of the stiffening. For relaxed actin gels, the stiffness of the networks increases with frequency in the form of a power law as $G \approx (-i\omega)^{3/4}$ (*15*, *22*, *23*). Given the inverse relationship between response and stiffness, this is consistent with the behavior of our model system either in the absence of motors or at high ATP concentrations (Figs. 2A and 3A). With the onset of nonequilibrium activity, however, the power law changed toward a slope of ½, which is consistent with the prediction for filaments under tension (*24*). The full frequency dependence (green curve in Fig. 3A) is derived in (*13*). This frequency dependence also rules out another possible explanation for the observed stiffening of the network, namely an increased cross-linking of actin by inactive myosin. Cross-links alone will not change the $\omega^{-3/4}$ frequency dependence (*22*, *25*). Thus, the increased stiffness seen in Fig. 3B is most likely the result of motor-induced tension in the network strands.

Given the presence of both cross-links and myosin minifilaments in our system, we expect that the myosins generate contractile tension in actin filaments between cross-link points (Fig. 4A). We find rates on the order of a fraction of a micrometer per second in the movement of probe particles (Fig. 4B), consistent with typical rates of myosin motility. This slow buildup of strain implies quasi-static elastic deformations that include network compression. Increased filament density would imply a local reduction of the solvent/buffer, just as squeezing a sponge expels liquid. Given the stochastic binding kinetics of the myosins, the minifilaments eventually let go, which results in a fast relaxation of the network strain (Fig. 4B). The rate at which the network can relax is determined by the dissipation due to the inflow of solvent

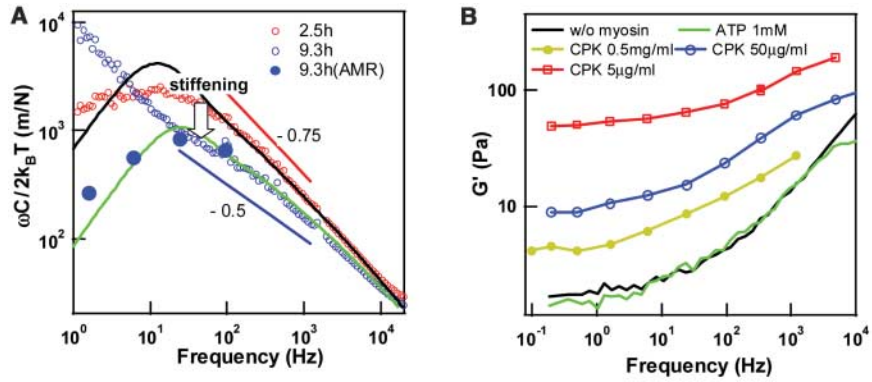

Fig. 3. Effect of filament tension on the response of the active networks (actin and myosin concentrations as in Fig. 1). (**A**) Spectra $\omega C(\omega)/2k_BT$ measured with PMR at 2.5 hours (open red circles) and 9.3 hours (open blue circles) and α'' measured with AMR at 9.3 hours (solid blue circles) after sample preparation (initial [ATP] = 3.5 mM). In the presence of nonequilibrium activity, the response function is reduced, indicating a stiffer sample, which can be fully accounted for by prestress/tension of filaments. Theoretical predictions (*13*) are shown for a network with filament tension of 0.1 pN, cross-link distance $l_c = 2.6$ μm (green curve), and no tension with the same l_c (black curve). Independently known parameters: friction coefficient $\zeta = 0.00377$ Pa·s, persistence length $l_p = 17 \times 10^{-6}$ m, probe radius $a = 2.5$ μm. (**B**) Shear modulus $G'(\omega)$ at controlled [ATP]: green line, 1 mM ATP, same as control (black line, no myosin). Lower [ATP] stabilized below ~60 μM by creatine phosphokinase (CPK): ochre line, [CPK] = 0.5 mg/ml; blue line, 50 μg/ml; red line, 5 μg/ml.

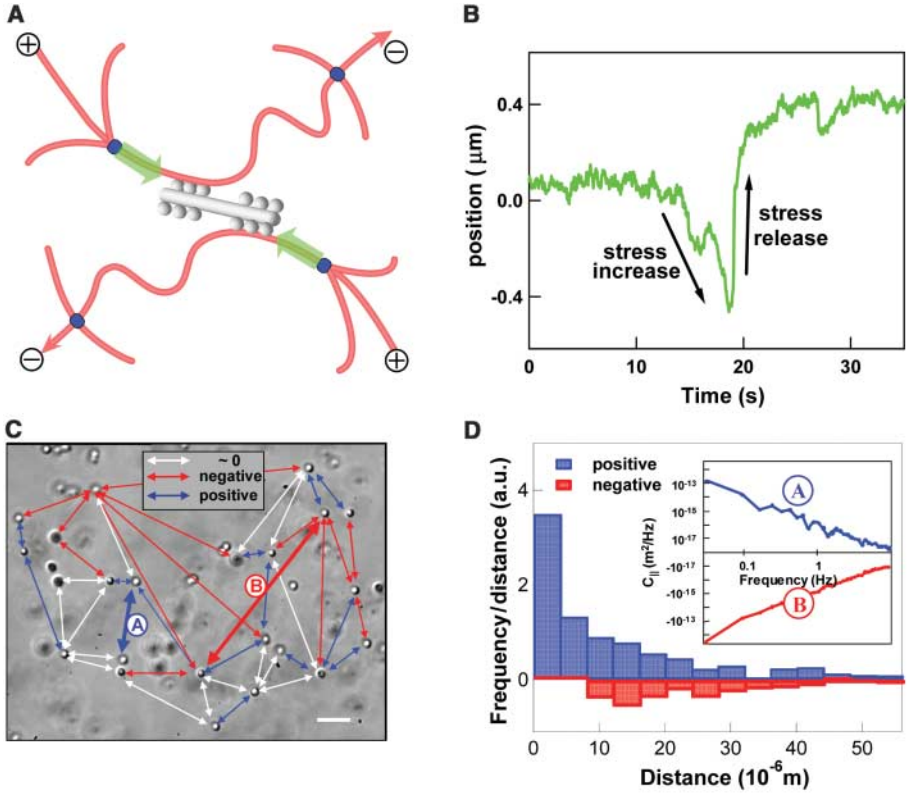

Fig. 4. (**A**) Schematic illustration of tension development in actin filaments (red). Myosin minifilaments (gray) cause network contraction between cross-links (blue). (**B**) Typical contractile event reflected in the motion of a probe particle. (**C**) Correlated motion of particle pairs (diameter 1.1 μm; scale bar, 5 μm) can be measured by video microscopy (*13*, *16*). In equilibrium, cross-correlations must be positive (*16*, *17*, *27*); nonequilibrium forces can lead to positive (blue arrows), negative (red arrows), or no correlations (white arrows). (**D**) Histogram of particle pairs showing positive (blue) and negative (red) correlations dependent on distance. The frequency (vertical axis) was normalized by distance to compensate for the increasing probability of finding a second bead at a given distance. Inset: representative cross-correlation spectra [particle pairs A and B in (C)] with positive (blue) and negative (red) correlations. Negative correlations are observed only at low frequencies, where nonequilibrium behavior is apparent in Fig. 2B.

(like the swelling of a sponge). Time scales for this process are expected to be on the order of $\eta(r/\xi)^2/G$ (*15*, *17*), where ξ (~0.3 μm) is the mesh size of the network and r is a typical length scale of deformation. If we take the cross-linking distance as r (~3 μm), this gives a relaxation time of ~0.1 s, which is consistent with the observed relaxation in Fig. 4B and the appearance of motor activity in Fig. 2B.

To further test the hypothesis that the nonequilibrium effects we observe are due to contractile/compressive gel deformations, we also examined the correlated motions of pairs of particles within the network (Fig. 4, C and D). The observed anticorrelations in particular are not expected in equilibrium, but they are consistent with the contractile forces sketched in Fig. 4A.

Thus, actin, myosin, and cross-links are sufficient to capture essential and general features of contractility and mechanical adaptation in cytoskeletal networks. These observations suggest mechanisms by which cells could rapidly modulate their stiffness by flexing their internal "muscles" without changing the density, polymerization, or bundling state of F-actin. Cells can actively adapt their elasticity to the mechanics of the extracellular matrix (*26*) or to an externally applied force (*1*), and motors could be the cause for that. From a materials perspective, this in vitro model system exhibits an active state of matter that adjusts its own mechanical stiffness via internal forces. This work can be a starting point for exploring both model systems and cells in quantitative detail, with the aim of uncovering the physical principles underlying the active regulation of the complex mechanical functions of cells.

References and Notes

1. P. A. Janmey, D. A. Weitz, *Trends Biochem. Sci.* **29**, 364 (2004).
2. A. Einstein, *Ann. Phys.* **17**, 549 (1905).
3. A. W. C. Lau, B. D. Hoffman, A. Davies, J. C. Crocker, T. C. Lubensky, *Phys. Rev. Lett.* **91**, 198101 (2003).
4. L. Le Goff, F. Amblard, E. M. Furst, *Phys. Rev. Lett.* **88**, 018101 (2002).
5. G. D'Anna, P. Mayor, A. Barrat, V. Loreto, F. Nori, *Nature* **424**, 909 (2003).
6. D. Bray, *Cell Movements: From Molecules to Motility* (Garland, New York, ed. 2, 2001).
7. G. Laevsky, D. A. Knecht, *J. Cell Sci.* **116**, 3761 (2003).
8. E. Reisler, C. Smith, G. Seegan, *J. Mol. Biol.* **143**, 129 (1980).
9. D. Humphrey, C. Duggan, D. Saha, D. Smith, J. Kas, *Nature* **416**, 413 (2002).
10. T. Hayashi, K. Maruyama, *J. Biochem. (Tokyo)* **78**, 1031 (1975).
11. L. A. Hough, H. D. Ou-Yang, *Phys. Rev. E* **65**, 021906 (2002).
12. D. Mizuno, Y. Kimura, R. Hayakawa, *Phys. Rev. Lett.* **87**, 088104 (2001).
13. See supporting material on *Science* Online.
14. T. G. Mason, D. A. Weitz, *Phys. Rev. Lett.* **74**, 1250 (1995).
15. F. Gittes, B. Schnurr, P. D. Olmsted, F. C. MacKintosh, C. F. Schmidt, *Phys. Rev. Lett.* **79**, 3286 (1997).
16. J. C. Crocker *et al.*, *Phys. Rev. Lett.* **85**, 888 (2000).
17. A. J. Levine, T. C. Lubensky, *Phys. Rev. Lett.* **85**, 1774 (2000).
18. M. L. Gardel *et al.*, *Science* **304**, 1301 (2004).
19. F. C. Mackintosh, J. Kas, P. A. Janmey, *Phys. Rev. Lett.* **75**, 4425 (1995).
20. C. Veigel *et al.*, *Nature* **398**, 530 (1999).
21. C. Storm, J. J. Pastore, F. C. MacKintosh, T. C. Lubensky, P. A. Janmey, *Nature* **435**, 191 (2005).
22. F. Gittes, F. C. MacKintosh, *Phys. Rev. E* **58**, R1241 (1998).
23. D. C. Morse, *Macromolecules* **31**, 7044 (1998).
24. A. Caspi, M. Elbaum, R. Granek, A. Lachish, D. Zbaida, *Phys. Rev. Lett.* **80**, 1106 (1998).
25. G. H. Koenderink, M. Atakhorrami, F. C. MacKintosh, C. F. Schmidt, *Phys. Rev. Lett.* **96**, 138307 (2006).
26. D. E. Discher, P. Janmey, Y. L. Wang, *Science* **310**, 1139 (2005).
27. M. Buchanan, M. Atakhorrami, J. F. Palierne, C. F. Schmidt, *Macromolecules* **38**, 8840 (2005).

28. We thank M. Atakhorrami, G. H. Koenderink, D. Pine, and D. A. Weitz for helpful discussions, and K. Vermeulen for sample preparation. Supported by the Deutsche Forschungsgemeinschaft Research Center for Molecular Physiology of the Brain (C.F.S.). This work is part of the research program of the Stichting voor Fundamenteel Onderzoek der Materie (FOM), which is funded by the Nederlandse Organisatie voor Wetenschappelijk Onderzoek (NWO).

Supporting Online Material

www.sciencemag.org/cgi/content/full/315/5810/370/DC1
Materials and Methods
SOM Text
Movies S1 to S4
References

28 August 2006; accepted 5 December 2006
10.1126/science.1134404

An Inward-Facing Conformation of a Putative Metal-Chelate–Type ABC Transporter

H. W. Pinkett,[1] A. T. Lee,[1] P. Lum,[1]* K. P. Locher,[2] D. C. Rees[1]†

The crystal structure of a putative metal-chelate–type adenosine triphosphate (ATP)–binding cassette (ABC) transporter encoded by genes *HI1470* and *HI1471* of *Haemophilus influenzae* has been solved at 2.4 angstrom resolution. The permeation pathway exhibits an inward-facing conformation, in contrast to the outward-facing state previously observed for the homologous vitamin B_{12} importer BtuCD. Although the structures of both HI1470/1 and BtuCD have been solved in nucleotide-free states, the pairs of ABC subunits in these two structures differ by a translational shift in the plane of the membrane that coincides with a repositioning of the membrane-spanning subunits. The differences observed between these ABC transporters involve relatively modest rearrangements and may serve as structural models for inward- and outward-facing conformations relevant to the alternating access mechanism of substrate translocation.

Transporters catalyze the thermodynamically unfavorable translocation of substrates against a transmembrane concentration gradient through the coupling to a second, energetically favorable process. One of the most widespread families of transporters, the adenosine triphosphate (ATP)–binding cassette (ABC) family (*1*–*4*), uses the binding and hydrolysis of ATP to power substrate translocation. ABC transporters are minimally composed of four domains, with two transmembrane domains (TMDs) and two ABCs or nucleotide-binding domains (NBDs) located in the cytoplasm. Although diverse with respect to physiological function and TMD architecture, ABC transporters are characterized by two highly conserved NBDs that contain critical sequence motifs for ATP binding and hydrolysis, including the P loop present in many nucleotide-binding proteins and the ABC signature or C-loop motif [Leu-Ser-Gly-Gly-Gln (LSGGQ)] that is specific to ABC transporters. These similarities suggest a common mechanism by which ABC transporters orchestrate a sequence of nucleotide- and substrate-dependent conformational changes that translocate the substrate across the membrane through interconversion of outward- and inward-facing conformations; this type of "alternating access" model has been generally found to provide a productive framework for the mechanistic characterization of transporters (*5*). For prokaryotic ABC transporters functioning as importers, substrate translocation is also dependent on high-affinity periplasmic-binding proteins (*6*) that deliver the ligand to the outward-facing state of the cognate transporter.

The HI1470/1 transporter from *Haemophilus influenzae* belongs to the family of binding protein–dependent bacterial ABC transporters that mediate the uptake of metal-chelate species, including heme and vitamin B_{12} (*7*). Because iron is often an essential nutrient, members of this family are widely distributed throughout bacteria, including pathogenic organisms such as *H. influenzae* (*8*). The molecular architecture for

[1]Division of Chemistry and Chemical Engineering, Howard Hughes Medical Institute, MC 114-96, California Institute of Technology (Caltech), Pasadena, CA 91125, USA. [2]Institute of Molecular Biology and Biophysics, ETH Zurich, 8093 Zurich, Switzerland.

*Present address: Department of Biological Sciences, University of Southern California, Los Angeles, CA 90089, USA.
†To whom correspondence should be addressed. E-mail: dcrees@caltech.edu